Altered Renal Distal Tubule Structure and Renal Na^+ and Ca^{2+} Handling in a Mouse Model for Gitelman's Syndrome

JOHANNES LOFFING,*† VOLKER VALLON,‡# DOMINIQUE LOFFING-CUENI,*† FINTAN AREGGER,* KERSTIN RICHTER,‡# LAURENCE PIETRI,§ MAY BLOCH-FAURE,§ JOOST G.J. HOENDEROP,‖ GARY E. SHULL,¶ PIERRE MENETON,§ and BRIGITTE KAISSLING*

Institute of Anatomy, University of Zurich, Zurich, Switzerland; †Department of Pharmacology and Toxicology, University of Lausanne, Lausanne, Switzerland; ‡Departments of Medicine and Pharmacology, University of California and VAMC, San Diego, California; §Institut National de la Santé et de la Recherche Medicale U367, Paris, France; ‖Department of Cell Physiology, University Medical Center Nijmegen, Nijmegen, The Netherlands; ¶Department of Molecular Genetics, University of Cincinnati, Cincinnati, Ohio; #Department of Pharmacology and Toxicology, University of Tuebingen, Tuebingen, Germany

Abstract. Gitelman's syndrome, an autosomal recessive renal tubulopathy caused by loss-of-function mutations in the thiazide-sensitive NaCl co-transporter (NCC) of the distal convoluted tubule (DCT), is characterized by mild renal Na^+ wasting, hypocalciuria, hypomagnesemia, and hypokalemic alkalosis. For gaining further insights into the pathophysiology of Gitelman's syndrome, the impact of NCC ablation on the morphology of the distal tubule, on the distribution and abundance of ion transport proteins along its length, and on renal tubular Na^+ and Ca^{2+} handling in a gene-targeted mouse model was studied. NCC-deficient mice had significantly elevated plasma aldosterone levels and exhibited hypocalciuria, hypomagnesemia, and compensated alkalosis. Immunofluorescent detection of distal tubule marker proteins and ultrastructural analysis revealed that the early DCT, which physiologically lacks epithelial Na^+ (ENaC) and Ca^{2+} (TRPV5) channels, was virtually absent in NCC-deficient mice. In contrast, the late DCT seemed intact and retained expression of the apical ENaC and TRPV5 as well as basolateral Na^+-Ca^{2+} exchanger. The connecting tubule exhibited a marked epithelial hypertrophy accompanied by an increased apical abundance of ENaC. Ca^{2+} reabsorption seemed unaltered in the distal convolution (*i.e.*, the DCT and connecting tubule) as indicated by real-time reverse transcription–PCR, Western blotting, and immunohistochemistry for TRPV5 and Na^+-Ca^{2+} exchanger and micropuncture experiments. The last experiments further indicated that reduced glomerular filtration and enhanced fractional reabsorption of Na^+ and Ca^{2+} upstream and of Na^+ downstream of the DCT provide some compensation for the Na^+ transport defect in the DCT and contribute to the hypocalciuria. Thus, loss of NCC leads to major structural remodeling of the renal distal tubule that goes along with marked changes in glomerular and tubular function, which may explain some of the clinical features of Gitelman's syndrome.

The renal distal convolution (DC), comprising the distal convoluted tubule (DCT) and the connecting tubule (CNT), plays an important role in the fine tuning of renal Na^+ and K^+ excretion. Moreover, it is the site of regulated transcellular Ca^{2+} and Mg^{2+} transport in the kidney [reviewed in (1,2)]. The thiazide-sensitive NaCl co-transporter (NCC) and the amiloride-sensitive epithelial sodium channel (ENaC) are the major apical Na^+ transport pathways in the DCT and in the CNT, respectively (1). In rodents (3,4) and humans (5), both are co-expressed in the late DCT. High amounts of Ca^{2+} transporting proteins such as the apical calcium channel (TRPV5/ECaC1) and the basolateral Na^+-Ca^{2+}-exchanger (NCX) have been revealed in the DCT and CNT [reviewed in (6,7)]. Likewise, proteins implicated in renal Mg^{2+} handling, such as the apical TRPM6 cation channel (8,9) and the basolateral γ subunit of the Na-K-ATPase (10), are highly expressed in the DC.

NCC loss-of-function mutations cause human Gitelman's syndrome, an autosomal recessive tubulopathy that is characterized by mild renal Na^+ wasting, hypocalciuria, hypomagnesemia, and hypokalemic alkalosis (11). Numerous NCC mutations, occurring throughout the entire coding sequence of the protein, have been described (12,13). When heterologously expressed in *Xenopus laevis* oocytes, mutated NCC proteins are retained in the endoplasmic reticulum (ER) (14,15) or do not exhibit normal NaCl cotransport activity when they reach

Received April 28, 2004. Accepted June 19, 2004.
Correspondence to Dr. Johannes Loffing, Department of Pharmacology and Toxicology, University of Lausanne, Rue du Bugnon 27, CH-1005 Lausanne. Phone: +41–21–692–53–68; Fax: +41–21–692–53–55; E-mail: johannes.loffing@ipharm.unil.ch
V.V. and D.L.-C. contributed equally to this work.
1046-6673/1509-2276
Journal of the American Society of Nephrology

DOI: 10.1097/01.ASN.0000138234.18569.63

the cell surface (14). Although the molecular and cellular mechanisms that lead to NCC dysfunction in Gitelman's syndrome are beginning to be understood, many aspects of the pathophysiologic mechanisms that lead to the characteristic phenotype of the disease are still elusive.

For example, compared with patients with other salt-losing tubulopathies (*e.g.*, pseudohypoaldosteronism type I), patients with Gitelman's syndrome have only mild renal Na^+ wasting and small, although significant, reduction in BP (16), pointing to yet not well-characterized renal adaptive mechanisms that allow compensation for impaired NCC-mediated NaCl reabsorption. Moreover, it is unclear how mutations of NCC affect the renal handling of divalent cations. Experiments on the acute effect of thiazides on microperfused DCT (17), on DCT cell vesicle preparation (18), and on immortalized DCT cells *in vitro* (19) pointed to increased Ca^{2+} transport by DCT cells in response to an acute inhibition of NCC function. On the basis of these experiments, it has been hypothesized that the hypocalciuria in Gitelman's syndrome is due to increased Ca^{2+} reabsorption by the DCT. Two mechanisms, neither of which has been proved, have been proposed to explain the hypocalciuria: (*1*) impaired NaCl entry *via* NCC may lower the intracellular chloride concentration, hyperpolarize the plasma membrane, and subsequently activate voltage-gated Ca^{2+} channels in the apical plasma membrane; and (*2*) reduced intracellular Na^+ may stimulate Ca^{2+} exit across the basolateral membrane as a result of increased activity of the basolateral NCX (20). The hypomagnesemia is even less readily explained. In DCT segments *in vivo* (21) and in immortalized DCT cells *in vitro* (22), inhibition of NCC by thiazides stimulates rather than inhibits Mg^{2+} transport by DCT cells. Therefore, it has been presumed that hypomagnesemia is not related to altered magnesium handling by the DCT itself but might be secondary to the hypokalemia in Gitelman's patients (22).

Schultheis *et al*. (23) generated an NCC null mutant mouse model that mimics to a large extent the renal phenotype of the disease. Like affected humans, these mutant mice exhibit hypocalciuria and hypomagnesemia with no apparent signs of hypovolemia as long as the animals are kept on a standard Na^+ intake (23). Ultrastructural analysis of kidneys from these mice revealed a sharp reduction in the number of morphologically identifiable DCT cells (23), but a detailed analysis of distal tubule segments and of the expression pattern of their major Na^+ and Ca^{2+} transporting proteins is still lacking. Such an analysis is essential as the various morphologically recognizable subsegments of the cortical distal tubule (the thick ascending limb [TAL], the early and late DCT, the CNT, and the cortical collecting duct [CCD]) differ markedly with respect to their ion transport proteins and also in their importance for renal handling of divalent cations [reviewed in (1,2,24,25)]. Moreover, specific pathogenetic mechanisms that may explain the characteristic phenotype of NCC deficiency have not yet been studied using this mouse model.

In the present study, we addressed the question of whether structural and functional changes in the distal tubule might provide compensation for the loss of NCC-mediated Na^+ transport and may explain the hypocalciuria. To accomplish this, we used a variety of techniques to determine the impact of NCC ablation on the structure of the distal tubule and the expression patterns of ion transport proteins along its lengths. We also investigated tubular Na^+ and Ca^{2+} handling and glomerular function. Our data point to a profound structural and functional remodeling of the distal nephron as well as changes in tubular and glomerular function that contribute to both the limitation of renal salt wasting and the altered renal Ca^{2+} handling in NCC-deficient mice.

Materials and Methods

Animals

Generation of homozygous NCC-deficient (NCC−/−) mice has been described previously (23). Heterozygous mice (NCC+/−) were backcrossed into a homogeneous genetic background of C57BL/6 mice (Iffa Credo, Arbresle, France) for >10 generations. Animals were bred in a standard, non-specific pathogen free (SPF) animal facility. Experiments were performed on 2- to 3-mo-old female and, for micropuncture experiments, male wild-type (NCC+/+) or null (NCC−/−) littermates. All animals had free access to standard lab diet (containing 0.24% Na^+) and tap water and were housed either in groups of six animals or individually in metabolic cages to allow recording of 24-h urinary volume and ion excretion. All experimental procedures were in accordance with the Guide for the Care and Use of Laboratory Animals (Institute of Laboratory Animal Resources, National Academy of Sciences, Bethesda, MD) and complied with the legal stipulations of the countries in which the experiments were performed.

Blood Analysis

For plasma K^+, Ca^{2+}, Mg^{2+}, and aldosterone measurements, mice were anesthetized by intraperitoneal administration of ketamine/xylazine (0.1 and 0.01 mg/g body wt, respectively). Blood was collected by puncture of the retrobulbar venous plexus. Plasma K^+ was measured by automated enzymatic methods (Kodak Biolyzer; Eastman Kodak, Rochester, NY). Plasma Ca^{2+} and Mg^{2+} were determined by atomic absorption spectrophotometry (model 3110; Perkin Elmer, Norwalk, CT). Plasma aldosterone concentration was measured by RIA (Kit Aldo RIA, Sanofi Diagnostics, Pasteur, France). Blood collected from retrobulbar venous plexus of awake mice was immediately analyzed for gases and pH.

Western Blot Analysis

Kidneys were homogenized in extraction buffer (250 mM sucrose, 150 mM NaCl, 30 mM Tris [pH 7.5], and 0.5 mM PeFabloc; Roche, Rotkreuz, Switzerland). Supernatants from two centrifugations at 1500 × *g* were pooled and centrifuged at 100,000 × *g* for 1 h. The pellet was resuspended in 100 μl of extraction buffer. Equal amounts of protein (~70 μg) from kidneys of wild-type and knockout mice were diluted in reducing sample buffer (4× NuPAGE-LDS; Invitrogen, Basel, Switzerland), heated for 10 min at 70°C, and loaded on a 4 to 12% polyacrylamide gel (Bis-Tris-Gels; NuPAGE; Invitrogen). After electrophoretic separation, proteins were transferred to a polyvinylidene difluoride membrane (BioRad, Reinach, Switzerland). The membrane was blocked for 30 min in 5% nonfat dry milk in a Tris-NaCl-Tween-Buffer (TNT) and was then incubated at 4°C for 16 h with either a rabbit anti-NCC antibody (26) or a rabbit anti-canine NCX (Swant, Bellinzona, Switzerland) antibody, each diluted 1:2000 in TNT buffer with 5% dry milk, followed by incubation for 2 to 3 h with a 1:2000 dilution of horseradish peroxidase–conjugated

goat anti-rabbit IgG. Sites of antibody binding were visualized with the ECL Western blotting analysis system (Amersham Pharmaceutica, Otelfingen, Switzerland).

Light and Electron Microscopy

The kidneys of anesthetized mice were fixed by vascular perfusion with 3% paraformaldehyde and 0.05% picric acid as described previously (27). Parts of the kidneys were postfixed for 24 h in the same fixative to which 1.0% glutardialdehyde was added. Afterward, the tissue was embedded in Epoxy resin (Epon). Semithin and ultrathin sections were cut with an ultramicrotome (Reichert Jung, Vienna, Austria) and stained with 1% methylene blue and 1% azure II, and lead citrate and uranyl acetate, respectively. Sections were studied with a Polyvar microscope (Reichert Jung, Vienna, Austria) and a Philips CM 100 electron microscope, respectively.

Immunohistochemistry

The remaining parts of the kidneys were frozen in liquid propane and processed for immunohistochemistry as described previously (27). The following primary antibodies were used: rabbit anti-rat bumetanide-sensitive Na-K-2Cl co-transporter (NKCC2) (28); rabbit anti-rat NCC diluted 1:8000; rabbit anti-rat α-subunit, β-subunit, and γ-subunit of ENaC (29) diluted 1:500 to 1:1000 ($\alpha\beta$ENaC) or 1:20,000 (γENaC); rabbit anti-rat parvalbumin (PV; Swant) diluted 1:2000; guinea pig anti-rabbit TRPV5 diluted 1:500 (30); rabbit anti-canine NCX (Swant) diluted 1:1000; rabbit anti-rat calbindin D28K (CB; Swant) diluted 1:20,000; mouse anti-chicken CB (Swant) diluted 1:40,000; and mouse anti-bovine H^+-ATPase (31) diluted 1:4. Binding sites of the primary antibodies were detected with Cy3-conjugated donkey anti-rabbit IgG (Jackson ImmunoResearch Laboratories, West Grove, PA), Cy3-conjugated goat anti–guinea pig (Jackson ImmunoResearch Laboratories), and FITC-conjugated goat anti-mouse IgG (Jackson ImmunoResearch Laboratories), diluted 1:1000, 1:500, and 1:40 in PBS/BSA 1%, respectively. For control of nonspecific antibody binding, the primary antibodies were omitted or replaced by a nonimmune rabbit serum.

Identification of Tubular Segments in Mice

Cortical distal tubular segments were identified according to immunohistochemical (Table 1) and standard morphologic criteria that are described elsewhere (25,32). The kidneys of nine mice per group (from two independent breedings) were histologically analyzed by three experienced investigators (J.L., D.L., B.K.), who were blinded to the genotype of the animals. Qualitative judgments regarding tubular morphology and immunostainings were similar for all investigators.

Morphometric Measurements

Consecutive cryosections were stained with polyclonal antibodies against PV, NCX, ENaC, and aquaporin 2 (AQP2). Each section was also co-stained with a monoclonal antibody against CB. Overviews were taken from each section with the $\times 10$ objective of a Polyvar microscope (Reichert-Jung) using a CDD camera. After printing of the micrographs, distal tubular segments were identified according to their specific antibody-staining pattern (Table 1). Because NCC expression, which was the primary characteristic of the DCT in wild-type mice, was absent in knockout mice, we defined the early DCT for both wild-type and knockout mice by the high abundance of PV and low, if any, NCX and CB immunostaining. The late DCT was defined by the presence of ENaC and by strong NCX and CB immunostaining. CNT were defined by coexpression of ENaC and AQP2, intermediate NCX and/or CB immunostaining, and their characteristic location within the cortical labyrinth. The CCD was classified by coexpression of ENaC and AQP2 but undetectable NCX and weak CB immunostaining. The fractional cortical tubular volumes for early DCT, late DCT, CNT, and CCD were determined from the printed micrographs by planimetric point-counting methods according to Weibel (33).

RNA Isolation and Quantitative PCR

Total RNA from kidney was isolated using Trizol Reagent (Life Technologies BRL, Life Technologies, Breda, The Netherlands) according to the manufacturer's protocol. RNA was treated with DNAse to prevent contamination of genomic DNA and finally resuspended in diethylpyrocarbonate-treated milliQ water. Total RNA (2 μg) was subjected to reverse transcription using Moloney Murine Leukemia Virus Reverse Transcriptase (Life Technologies BRL) as described previously (34). Expression levels of renal TRPV5, calbindin-D_{28K}, and NCX1 mRNA were quantified by real-time quantitative PCR, using the ABI Prism 7700 Sequence Detection System (PE Biosystems, Rotkreuz, Switzerland). With the use of standard curves, the amount of copy numbers of the target genes in each sample was

Table 1. Segmental distribution of proteins used for the identification of tubular segments in C57BL/6 mice[a]

	TAL	DCT early	DCT late	CNT	CCD
NKCC2	+++				
NCC		+++	++		
ENaC			+	+++	+++
AQP2				++	+++
TRPV5			+++	++	
NCX		+	+++	++	
CB		+	+++	++	++
PV[b]		+++			

[a] Protein abundance: + weak; ++ intermediate; +++ strong; TAL, thick ascending limb; DCT, distal convoluted tubule; CNT, connecting tubule; CCD, cortical collecting duct; NKCC2, Na^+-K^+-$2Cl^-$ Cotransporter 2; NCC, Na^+-Cl^- Cotransporter; ENaC, epithelial Na^+ channel; TRPV5, transient receptor potential, vanilloid-receptor related ion channel 5; NCX, Na^+-Ca^{2+} exchange; CB, calbindin D28k; PV, parvalbumin.

[b] Rarely, weak PV immunostaining is also present in TAL and late DCT cells, whereas strong PV immunostaining is always visible in early DCT cells. These observations are consistent to two previous studies on C57BL/6 mice (27) (9), but are at variance to reports on NMRI mice that described high levels of PV in both early and late DCT (54).

calculated and expressed as a ratio to the hypoxanthine-guanine phosphoribosyl transferase gene. Primers and probes targeting the genes of interest were designed using Primer Express software (Applied Biosystems, Foster City, CA) as described previously (35).

Clearance and Micropuncture Experiments

Mice were prepared for micropuncture under inactin/ketamine anesthesia as described (36). For assessment of GFR of both kidneys and of single nephrons, [^{3}H]inulin was infused intravenously. Urine collections were performed using a bladder catheter. The left kidney was prepared for micropuncture. On the kidney surface, the last loop of proximal tubules (LPT) or the DC were identified and punctured for quantitative collections of tubular fluid. Tubular fluid volumes were determined from column length in a constant bore capillary. The concentrations in tubular fluid of Na^+ and K^+ were determined by a microflame photometer (Department of Pharmacology, University of Tübingen, Germany) (36) and of Ca^{2+} by a flow-through microfluorometer (NanoFlo; WPI, Sarasota, FL) using Fluo-3 (MoBiTec, Göttingen, Germany) for detection (37).

Statistical Analyses

Data are given as means ± SEM. Statistical differences between means were evaluated by unpaired *t* test (two tails). Differences were considered to be significant at $P < 0.05$.

Results

Physiologic Data

As previously reported (23), NCC−/− mice exhibited hypocalciuria and hypomagnesemia (Table 2). Moreover, the animals had a mild compensated alkalosis as indicated by the increased plasma bicarbonate concentration. Plasma levels for potassium did not differ between NCC+/+ and NCC−/− mice. Plasma aldosterone levels were significantly elevated when compared with NCC+/+ mice. This is at variance with the initial characterization of NCC−/− mice (23) and might be related to differences in the genetic background (mixed and C57BL/6 in the previous and the present study, respectively) or animal husbandry.

Lack of NCC Protein in Kidneys of NCC−/− Mice

To confirm the absence of NCC protein from the kidneys of NCC−/− mice, we performed Western blot analysis and immunohistochemistry with affinity-purified anti-NCC IgG. In NCC+/+ mice, Western blot analysis of kidney homogenates revealed a single band at 190 kD and occasionally weaker additional bands at higher molecular weights, likely representing multimeric NCC complexes (Figure 1a); none of the bands was detectable in NCC−/− mice (Figure 1a). In immunohistochemical experiments with the NCC antiserum, a number of tubular profiles were brightly stained in the renal cortex of NCC+/+ mice but not in kidney sections of NCC−/− mice (Figure 1b).

Table 2. Plasma parameters of NCC+/+ (n = 12) and NCC−/− (n = 12) mice

	NCC+/+	NCC−/−
Potassium (mmol/l)	4.4 ± 0.3	4.3 ± 0.2
Calcium (mmol/l)	1.76 ± 0.05	1.71 ± 0.03
Magnesium (mmol/l)	1.05 ± 0.11	0.72 ± 0.09[a]
pH	7.33 ± 0.06	7.37 ± 0.04
Bicarbonate (mmol/l)	21.3 ± 1.9	25.7 ± 1.7[a]
Aldosterone (pg/ml)	657 ± 71	1917 ± 137[a]

[a] $P < 0.01$.
Values are means ± SEM.

Distribution of Transport Proteins and Structure along the Cortical Distal Nephron

The binding patterns of the antibodies that were used and the structure along the distal nephron of kidney sections of NCC+/+ mice were identical to those described previously (27). Loss of NCC had no apparent effect on TAL cell structure and NKCC2 abundance. In mice of both genotypes, NKCC2 immunostaining was visible in the apical plasma membrane of TAL cells and ceased abruptly at the transition from TAL to DCT (Figure 2).

In NCC+/+ mice, the abrupt termination of NKCC2 and the beginning of NCC expression coincided with a marked rise in epithelial height and strong cytoplasmic PV expression that extended for a considerable length along the DCT. In overviews of the renal cortex, a number of PV-positive tubular profiles were consistently visible in NCC+/+ mice (Figure 2, a and d) but almost absent in NCC−/− mice (Figure 2, b and f). In NCC−/− mice, the epithelium after the point at which NKCC2 expression terminated remained as thin as that of the preceding TAL, and immunostainings revealed none of the

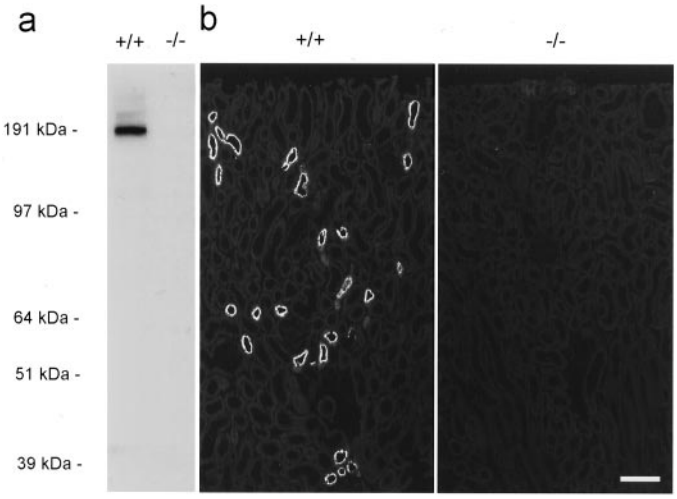

Figure 1. NaCl-co-transporter (NCC) protein abundance in kidneys of wild-type and NCC knockout mice. (a) Total kidney homogenates of wild-type (+/+) and knockout (−/−) mice were subjected to SDS-PAGE analysis and incubated with an affinity-purified rabbit anti-mouse NCC antibody, followed by a horseradish peroxidase–coupled donkey anti-rabbit IgG and subsequent ECL detection. (b) Cryosections; overviews of renal cortex of wild-type (+/+) and knockout mice (−/−) immunostained with an affinity-purified rabbit anti-mouse NCC antibody, followed by a Cy3-conjugated goat anti-rabbit IgG. Bar = ~200 μm.

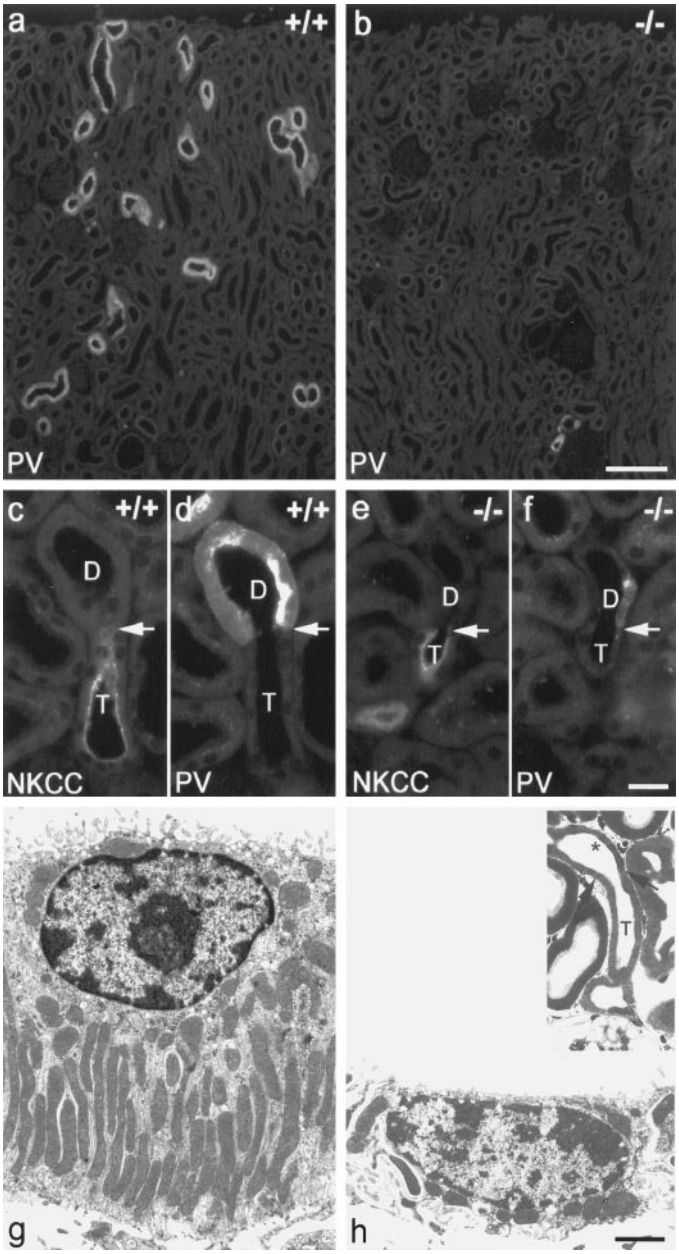

Figure 2. Early distal convoluted tubules (DCT) in the renal cortex of wild-type (+/+) and NCC knockout (−/−) mice. (a through f) Cryosections. (g and h) Epon thin sections. (a and b) Overviews of the kidney cortex immunostained by a polyclonal rabbit anti-rat parvalbumin (PV) antiserum followed by a Cy3-conjugated goat anti-rabbit IgG. (c through f) Transitions from thick ascending limb (TAL) to early DCT shown in consecutive cryosections (c and d, and e and f) stained either by a rabbit anti-rat Na-K-2Cl co-transporter (NKCC) antiserum or by a rabbit anti-rat PV antiserum, followed by a Cy3-conjugated goat anti-rabbit IgG; bright apical NKCC2 immunostaining characterizes the TAL (T) and ceases abruptly (arrows) at the transition to the early DCT (D), exactly where PV immunolabeling starts. (g and h) Electron microscopic images of early DCT cells from wild-type (+/+) and knockout (−/−) mice; transitions from TAL (T) to DCT (arrows) were identified on semithin sections (insert in h) and analyzed at the electron microscopic level in the successive ultrathin section. The DCT cell shown in h is marked by an asterisk in the insert. In wild-type mice, the early DCT cells are conspicuous by the dense alignment perpendicular to the basement membrane of elongated mitochondrial profiles, narrowly enveloped by basolateral plasma membranes. The cell nucleus is located on top of the row of mitochondria, just below the apical plasma membrane (g). In knockout mice, the height of the early DCT cells is approximately one third that of the cells in wild-type mice, with only a few mitochondria, basolateral plasma membrane infoldings, or apical microprojections (h). Bars = ~200 μm in b, ~20 μm in f, ~2 μm h.

tested proteins, except occasional minute amounts of PV and/or CB (Figures 2f and 3). The cells in this short tubular portion were analyzed further by electron microscopy. The cells revealed a pronounced structural atrophy when compared with the early DCT cells of NCC+/+ mice (Figure 2, g and h). In NCC−/− mice, intercalated cells, identified by their bright immunofluorescent staining with antibodies against the H^+-ATPase, were consistently found in close proximity to the transition from TAL to DCT (Figure 3, g and h). This is in contrast to wild-type animals, in which the most proximal intercalated cells appear distant from the TAL-DCT transition. Taken together, the findings from immunostaining and morphology studies suggest that the early DCT of knockout mice is drastically atrophied and shortened.

Intact Late DCT in NCC Knockout Mice

The short, hypoplastic early DCT segment in knockout mice abruptly transitions to a high epithelium (Figures 3 and 4) with cell nuclei in an apical position and with numerous mitochondria (Figure 4b). By immunostaining, these cells exhibited weak expression of ENaC (Figure 3b) and high expression of TRPV5 (Figures 3d and 4d) and CB (Figures 3f and 4, a, c, and e). AQP2 was detected only in the very last cells of this tubular portion (Figure 4, e and f). A few intercalated cells, apparent as unstained dark spots within the brightly CB-immunostained epithelium (Figure 5e), were observed consistently. By these collected features, the epithelium corresponded to the late DCT in wild-type mice. In knockout mice, it showed no apparent signs of structural atrophy.

Hypertrophied CNT in NCC Knockout Mice

The late DCT of knockout mice is followed by a tubular portion that corresponded by its antibody staining pattern and histotopographic localization to the CNT in wild-type mice (Table 1, Figures 5 and 6). In comparison with wild-type mice, CNT profiles from knockout mice revealed a marked epithelial hypertrophy (Figure 6, a and b) that was accompanied by an increased apical abundance of all three ENaC subunits, suggesting enhanced Na^+ transport rates. In wild-type mice, α-, β-, and γENaC subunits were seen almost exclusively in the cytoplasm of CNT cells, whereas in knockout mice, they were shifted toward the apical plasma membrane as shown exemplary for βENaC in Figure 6, c and d. The apical translocation of α-, β-, and γENaC was limited to the CNT and not visible in the CCD of NCC knockout mice as visible for γENaC in Figure 5f.

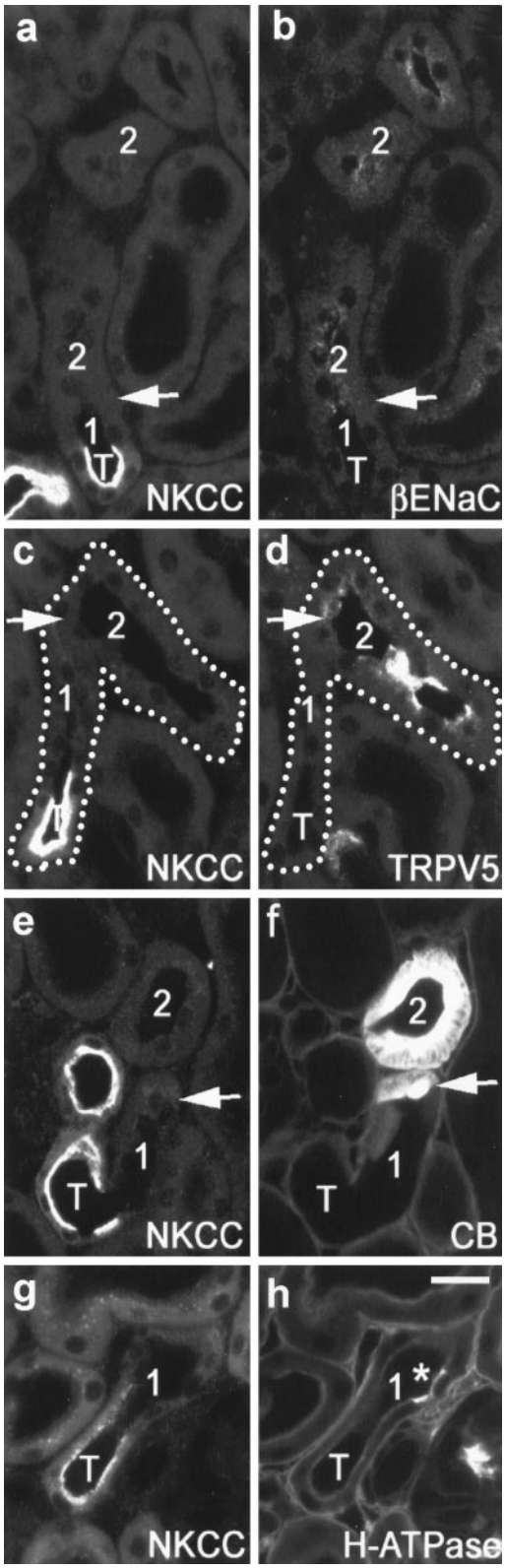

Figure 3. TAL-DCT transition in NCC knockout mice. Cryosections immunostained with rabbit antisera against rat NKCC2 (NKCC), rat β-subunit of the epithelial sodium channel (βENaC), affinity-purified guinea pig antiserum against epithelial Ca^{+} channel 1 (TRPV5), mouse monoclonal antibodies against calbindin D28k (CB), and the vacuolar H^{+}-ATPase (H-ATPase). a and b, c and d, and e and f are consecutive sections. (g and h) Double immunostaining on same section. Bright apical NKCC2 immunostaining (left column, a, c, e, and g) characterizes the TAL (T) and stops abruptly at the transition to the early DCT (1). The TAL is followed by a very short tubular portion, which exhibits no detectable ENaC or TRPV5 immunolabeling and only weak CB immunolabeling. The late DCT (2) is characterized by weak ENaC, strong TRPV5, and strong CB immunostaining. Note the rise in epithelial height (arrows) at the transition from early (1) to late (2) DCT. One intercalated cell, revealed by its high expression of H^{+}-ATPase, is seen in close proximity to the NKCC2-positive TAL. Immunofluorescent labeling of tubular basement membranes and interstitial cells in f and h is due to binding of the secondary FITC-labeled anti-mouse IgG to endogenous mouse immunoglobulins. Bar = ~20 μm

Morphometry

The fractional cortical tubular volumes of the early DCT, the late DCT, the CNT, and the CCD in wild-type and knockout mice (Figure 6) were consistent with the above-described qualitative observations. In knockout mice, the fractional volume for the early DCT was drastically lower than in wild-type mice. The fractional volumes of the late DCT were similar in both genotypes. The fractional volume of the CNT was significantly greater in knockout mice than in wild-type mice. The CCD volume was similar for mice of both genotypes. Although not specifically addressed in the present study, the morphologic changes along the CNT most likely comprise epithelial hypertrophy and hyperplasia. Numerous previous studies revealed that cellular hypertrophy and hyperplasia both contribute to the adaptation of the distal nephron to an enhanced tubular workload [reviewed in (1,25)].

Abundance of Ca^{2+} Transporting Proteins

The expression of TRPV5 and NCX mRNA, as well as the protein abundance of NCX, was not different between wild-type and NCC-deficient mice (Figure 7). Consistent with previous studies (26,34,37), TRPV5 could not be revealed by Western blot analysis of kidney homogenates, perhaps because of the comparably low abundance of the channel in total kidney preparations. Immunofluorescence revealed a slightly decreased abundance of TRPV5 and NCX along the luminal and basolateral membrane, respectively, of late DCT and CNT of NCC –/– mice that became most apparent at high antibody dilutions (Figure 7c). The lowered TRPV5 and NCX abundance in individual late DCT and CNT cells may explain the unchanged expression levels of TRPV5 and NCX in total kidney homogenates despite the significant hypertrophy of the CNT in NCC-deficient mice.

Clearance and Micropuncture Experiments

NCC−/− mice presented normal mean arterial BP but lower GFR and as a consequence lower glomerular filtration of Na^{+}, K^{+}, and Ca^{2+} than in NCC+/+ mice (Table 3). The lowered GFR but unaffected fractional whole kidney tubular reabsorption of Na^{+} and Ca^{2+} (Figure 8) resulted in a modestly reduced urinary excretion of Na^{+} and Ca^{2+} in NCC−/− mice compared with NCC+/+ mice (Table 3). Under balanced conditions when urinary Na^{+} excretion reflects body Na^{+} intake, it

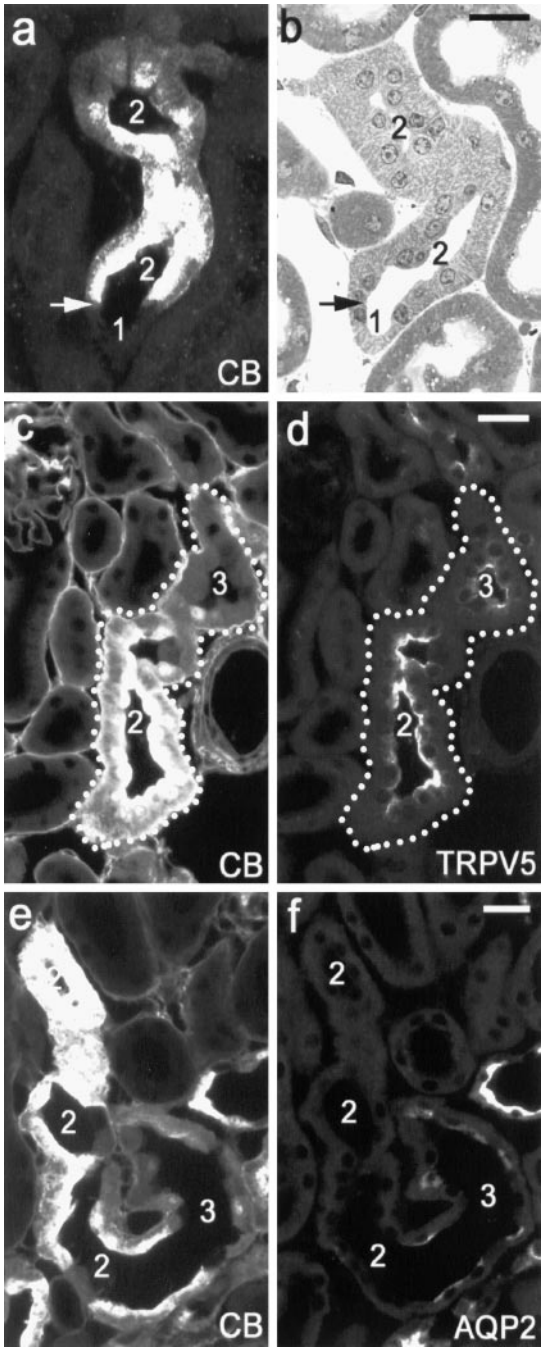

Figure 4. Immunofluorescent (a, c through f) and morphologic (b) characterization of late DCT in NCC knockout mice. (b) Epon semithin section; all others are cryosections immunostained with rabbit antisera (a) and mouse monoclonal antibodies (c and e) against CB, affinity-purified guinea pig antiserum against TRPV5 (d), or affinity-purified rabbit anti-rat aquaporin-2 (AQP; f). c and d, e and f are double immunostainings; the transition (arrows in a and b) from early (1) to late (2) DCT is characterized by the sharp increase in CB immunostaining and in the epithelial cell height (a and b). The late DCT (2) has high cytoplasmic CB (a, c, and e) and apical TRPV5 expression (d) but lacks detectable AQP2 along most of its lengths (f). Only at the transition from late DCT (2) to CNT (3), single cells express high CB levels and AQP2 (f), consistent with previous findings in wild-type mice showing that the very last NCC-positive DCT cells coexpress AQP2 [see Figure 3 in (25)]. The distally localized connecting tubule (3) exhibits weaker CB and TRPV5 expression than the preceding DCT portion and shows easily detectable AQP2. The labeling of tubular basement membranes and interstitial cells in c and e is due to binding of the secondary FITC-labeled anti-mouse IgG to endogenous mouse immunoglobulins. Bars = ~20 μm.

is expected that urinary Na^+ excretion is not different between NCC−/− and NCC+/+ mice. Thus, the neurohumoral activation associated with anesthesia and surgery may have induced a modestly greater renal Na^+ retention in NCC−/− mice. This could be the consequence of the documented CNT enlargement that may have created a Na^+ transport machinery in the CNT of NCC−/− mice that is more responsive to neurohumoral stimulation. Micropuncture experiments confirmed that single-nephron GFR was lower in NCC−/− than in NCC+/+ mice in collections from both the last loop of the proximal tubule on the kidney surface (LPT; 5.4 ± 0.2 *versus* 6.7 ± 0.4 nl/min; $P < 0.05$) and DC (5.2 ± 0.4 *versus* 6.7 ± 0.4 nl/min; $P < 0.05$). As depicted in Figure 8, fractional delivery of fluid, Na^+, K^+, and Ca^{2+} to the LPT were reduced, and thus fractional reabsorption up to this site increased in NCC−/− compared with NCC+/+ mice. Fractional delivery of fluid and Na^+ remained reduced in NCC−/− *versus* NCC+/+ mice up to the DC, whereas the fractional delivery of K^+ and Ca^{2+} to this site was not different between genotypes. The lower fractional delivery of Na^+ but constant fractional delivery of K^+ to the DC puncture sites resulted in a raised K^+ to Na^+ ratio in the tubular fluid in the DC of NCC−/− mice (Figure 9). These findings and the persistently greater K^+ to Na^+ ratio in the urine of NCC−/− than in NCC+/+ mice point to an enhanced functional activation of the aldosterone-sensitive distal nephron in NCC−/− mice (Figure 9).

Because K^+ secretion and Na^+ reabsorption occur along the distal nephron sites accessible to micropuncture (together with water reabsorption in CNT and CCD), the distal luminal K^+ to Na^+ ratio was used as an indicator of the distal collection site (Figure 10). Consistent with intact Ca^{2+} reabsorption along DC and confirming previous experiments that related fractional Ca^{2+} delivery in DC to luminal K^+ concentration (37), both NCC+/+ and NCC−/− mice showed a rapid fall in fractional Ca^{2+} delivery with increasing ratios of K^+ to Na^+ (Figure 10). The shift of the curve to the right in NCC−/− mice may reflect the greater functional activation of the aldosterone-sensitive distal nephron upstream from the puncturing sites. Consistent with some Ca^{2+} reabsorption between late DC accessible to micropuncture and urine, fractional deliveries of Ca^{2+} in late DC (high K^+ to Na^+ ratio) were modestly higher than values found in urine for both genotypes.

Discussion

In this study, we used morphologic, biochemical, and functional techniques to determine the impact of genetic NCC ablation on the morphology and the function of the renal distal tubule. Our data reveal a pronounced epithelial remodeling of the DCT and CNT in NCC-deficient mice that likely reflects

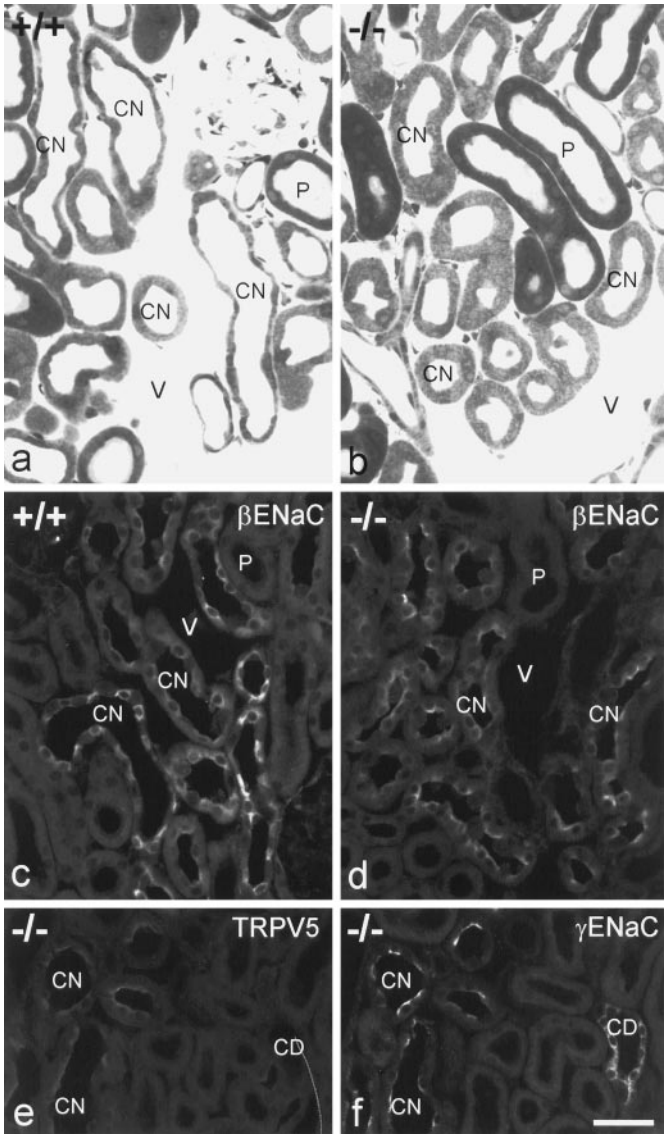

Figure 5. Connecting tubules (CN) in wild-type (+/+) and NCC knockout (−/−) mice. (a and b) Epon semithin sections. (c through f) Cryosections immunostained by rabbit anti–β-, anti-γENaC antisera or guinea pig anti-TRPV5 antibodies followed by a Cy3-conjugated goat anti-rabbit IgG and goat anti–guinea pig IgG, respectively. In mice of both genotypes, CN profiles are typically arranged around the cortical radial vessels (V) and therefore are clearly distinguished from collecting ducts (CD) that are running in the medullary rays at some distance from the cortical radial vessels (1,32). (a and b) CN cells are much taller in knockout than in wild-type mice. (c and d) In wild-type mice, ENaC is diffusely distributed throughout the cytoplasm of the CN cells; in NCC-deficient mice, ENaC is shifted toward the apical plasma membrane of the CN cells. (e and f) In the NCC−/− mice, apical translocation of ENaC is seen in TRPV5-positive CN cells but not in the TRPV5-negative CD cells. Unstained cells in CN and CD profiles are intercalated cells. V, cortical radial vein; P, proximal tubules. Bar = ~50 μm.

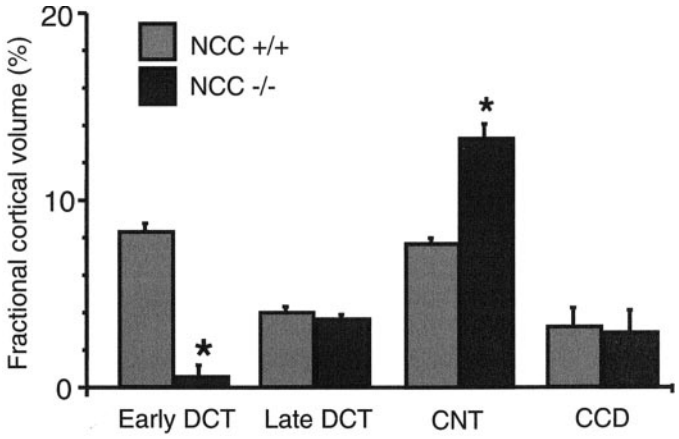

Figure 6. Fractional cortical volumes of early DCT, late DCT, CNT, and CCD in wild-type (+/+) and in NCC-deficient (−/−) mice. Distal tubule segments were identified as described in Materials and Methods. The fractional cortical tubular volumes were determined by the point-counting method, according to Weibel (33). Values are means ± SEM from four individual mice in each group. *$P < 0.05$ *versus* NCC +/+ values.

altered sodium transport activities in the respective segments. Moreover, our data suggest that altered renal Na^+ handling upstream and downstream of the DCT provides compensation for the Na^+ transport defect in the DCT and that hypocalciuria in NCC-deficient mice is primarily the consequence of altered renal Ca^{2+} handling upstream of the DCT.

Numerous studies, particularly on the renal DCT, revealed the close interrelationship between transepithelial ion transport activity and epithelial structure [reviewed in (1,32)]. Prolonged increases in NaCl transport rates in the DCT epithelium are followed by a notable epithelial hypertrophy, whereas a prolonged decrease in transport rates leads to DCT hypotrophy with reductions of mitochondrial volume and basolateral membrane area (1,32). In NCC-deficient mice, the alterations in epithelial structure of the DCT are compatible with those that result from markedly reduced transepithelial transport rates. We found a decrease in the fractional cortical tubular volume for the entire DCT (early and late parts) from ~13% in wild-type mice to ~4.5% in knockout mice. This reduction in fractional volume matches well the ~60% decrease of DCT cell number as detected previously by electron microscopic analysis (23). Remarkably, the atrophy of the DCT is limited to its early portion, which is almost absent from the kidneys of NCC−/− mice. In contrast, the late DCT of NCC−/− mice seems structurally intact and retains its typical DCT cell morphology and, with the exception of the NCC, the expression of ion transport proteins. This is consistent with our previous findings in thiazide-treated rats. In these rats, only the early DCT but not the late DCT undergoes apoptosis in response to NCC inhibition by thiazide treatment (38). The presence of additional ion transporters (*e.g.*, ENaC and TRPV5 and possibly others) may enable the late DCT cells to escape the detrimental effect of the genetic or pharmacologic loss of NCC function.

Although ~5% of the filtered sodium load is thought to be reabsorbed in the DCT by NCC, NCC-deficient mice show only little, if any, renal salt wasting (23). As long as the mice are kept on a sufficient Na^+ intake, the BP remains in the normal range and the mice show no apparent signs of hypo-

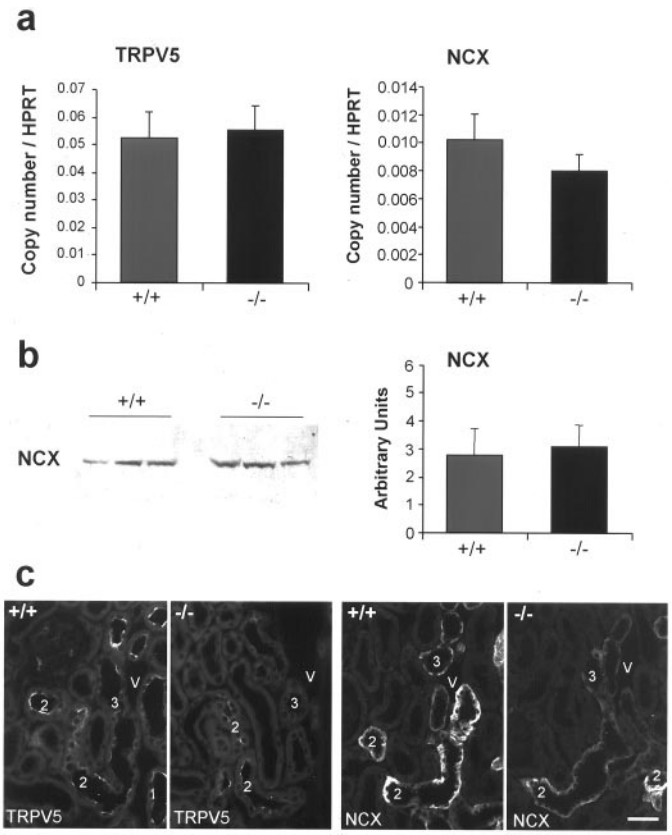

Figure 7. Expression of TRPV5 and NCX in kidneys of wild-type (+/+) and in NCC-deficient (−/−) mice. (a and b) Total kidney homogenates of wildtype (+/+) and knockout (−/−) mice were analyzed by real-time reverse transcription–PCR (RT-PCR; a) and SDS-PAGE (b) for the expression of TRPV5 and NCX at the mRNA and protein level, respectively. The copy numbers of the target genes analyzed by real-time RT-PCR were calculated and expressed as a ratio to the hypoxanthine-guanine phosphoribosyl transferase (HPRT) gene expression. Values are means ± SEM from five (a) and three (b) individual mice in each group. (c) Cryosections immunostained by guinea pig anti-TRPV5 and rabbit anti-NCX antibodies followed by a Cy3-conjugated goat anti-rabbit IgG and goat anti–guinea pig IgG, respectively. Apical TRPV5 and basolateral NCX immunostainings decrease from late DCT (2) to CNT (3) in mice of both genotypes. The intensity of the immunostainings is slightly stronger in NCC+/+ than in NCC−/− mice. Note that the used antibody dilution for TRPV5 was three times higher than that used for the immunostainings shown in Figures 3 and 4. Bar = ~50 μm.

volemia (23). Only the threefold elevation of plasma aldosterone levels, as seen in the present study, point to some degree of extracellular volume depletion. Likewise, patients with Gitelman's syndrome have been reported either to be normotensive (39) or to have comparably mild reductions in arterial BP (16). This indicates that mice and humans are able to compensate, at least partly, for the loss of NCC-mediated Na^+ transport. Our data suggest that two mechanisms, localized upstream and downstream of the DCT, contribute to this compensated phenotype. First, a lowered GFR and enhanced fractional proximal reabsorption reduce the tubular salt load delivered to the DC and, second, enhanced Na^+ reabsorption in the CNT recovers Na^+ that has not been reabsorbed in the preceding DCT.

The reduced GFR in NCC knockout mice is consistent with previous micropuncture and microperfusion studies that reported a decline in the GFR in response to pharmacologic inhibition of NCC by chlorothiazide (17,40). The reason for the reduced GFR in response to genetic or pharmacologic ablation of NCC function is unclear. It is probably not related to a direct activation of the tubuloglomerular feedback mechanism, because the primary Na^+ transport defect lies downstream of the macula densa. Also extracellular volume depletion cannot account for the significant drop in GFR. The BP of NCC-deficient and wild-type mice did not differ significantly in the present study or in a previous study (23). Likewise, thiazide diuretics reduce the GFR even when extracellular volume depletion is prevented by intravenous replacement of salt and fluid losses (17). Whatever the underlying mechanism is, the reduced GFR seems not to be sufficient to compensate fully for the NCC loss, because aldosterone-dependent stimulation of ENaC-mediated sodium transport seems to contribute as well. Knepper's group (41) showed by immunoblotting-techniques that the abundance of a lower molecular weight form of the γ-subunit of ENaC is increased in kidneys of NCC−/− mice, whereas the abundances of the major apical sodium transporting proteins of the proximal tubule and the TAL (NHE3 and NKCC2, respectively) are unchanged. The low molecular weight form of γENaC has been proposed to be indicative of enhanced ENaC activity and to represent γENaC subunits cleaved by luminal proteases (42). The observed hypertrophy of the CNT, the increased apical localization of ENaC along the CNT, and the enhanced Na^+-K^+ exchange along the DC establish that ENaC-mediated Na^+ reabsorption in the CNT is increased in the kidneys of NCC-deficient mice. The elevated plasma aldosterone levels most likely play a role in these adaptive changes in the CNT. Aldosterone stimulates Na^+ transport in the renal collecting system (43), induces CNT and CD cell hypertrophy [*e.g.*, (44,45)], shifts ENaC from intracellular compartments to the apical plasma membrane (42,46), and stimulates Na^+ and K^+ exchange in the CNT and CD (43). Surprising, we found no morphologic evidence for enhanced ENaC activity in the collecting ducts of NCC−/− mice. In mice of both genotypes, ENaC subunits were predominately localized at intracellular sites of CCD cells, and the fractional CCD volume did not differ between wild-type and NCC-deficient mice. These morphologic data do not exclude a stimulation of ENaC in the CCD, but they are consistent with previous patch-clamp (47), ion transport (48–50), and immunohistochemical (4,46) studies that revealed a several-times higher sodium transport rate and apical activity/abundance of ENaC in the CNT than in the CCD. The salient importance of nephron portions upstream of the CD for the maintenance of sodium homeostasis was highlighted by the recent development of mice with a targeted inactivation of αENaC only in the CD but not in the CNT and late DCT (51). Unlike mice and humans with generalized inactivation of ENaC, these mice are able to maintain Na^+ homeostasis even when challenged by sodium restriction (51).

Table 3. Blood pressure, glomerular filtration and urinary excretion of NCC+/+ (n = 7) and NCC−/− (n = 7) mice

	NCC+/+	NCC−/−
Body wt (g)	27.2 ± 0.5	28.0 ± 0.6
Mean arterial pressure (mmHg)	99 ± 3	97 ± 3
GFR (μl/min/g bw)	6.0 ± 0.5	4.3 ± 0.3[a]
Na^+-filtered (μmol/min/g bw)	0.91 ± 0.09	0.66 ± 0.04[a]
K^+-filtered (nmol/min/g bw)	38 ± 3	26 ± 3[a]
Ca^{2+}-filtered (nmol/min/g bw)	11.0 ± 0.1	7.6 ± 0.6[a]
Urinary flow (nl/min/g bw)	79 ± 14	52 ± 8
Urinary Na^+ excretion (nmol/min/g bw)	5.5 ± 1.1	2.9 ± 0.6[a]
Urinary K^+ excretion (nmol/min/g bw)	8.6 ± 1.1	6.7 ± 0.7
Urinary Ca^{2+} excretion (pmol/min/g bw)	29 ± 7	12 ± 3[a]

[a] $P < 0.05$.
Values are means ± SEM.

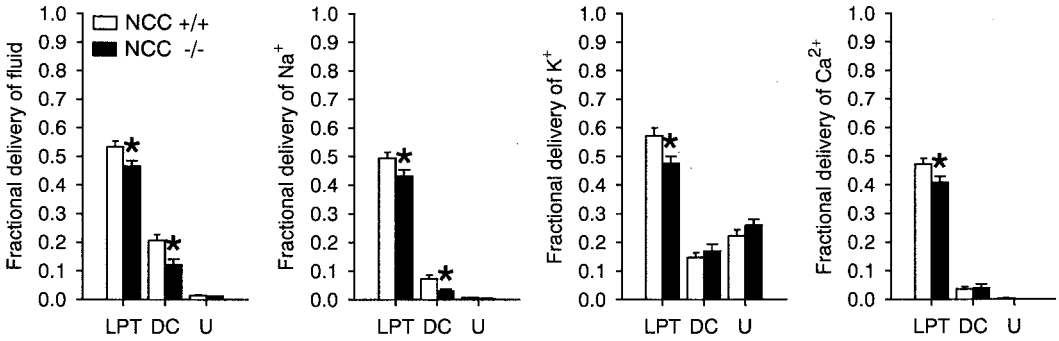

Figure 8. Fractional delivery of fluid, Na^+, K^+, and Ca^{2+} to the last surface loop of proximal tubule (LPT), distal convolution (DC), or urine (U) in NCC+/+ and NCC−/− mice. Values are means ± SEM from seven mice (U), 29 to 34 nephrons (LPT), or six to nine nephrons (DC) per group. *$P < 0.05$ *versus* NCC+/+ values.

Sodium transport via ENaC is electrogenic and coupled to K^+ secretion *via* luminal K^+ channels such as ROMK. In fact, conditions of an increased ENaC activity (*e.g.*, hyperaldosteronism) are often associated with renal K^+ losses (43). Likewise, patients with Gitelman's syndrome frequently develop hypokalemia that can be corrected by treatment with mineralocorticoid-receptor antagonists (52). Despite the apparent hyperaldosteronism and the activation of ENaC, NCC-deficient mice have normal plasma K^+ levels. The reason for the absence of hypokalemia is unclear but could be related to species differences in distal nephron potassium handling or to a comparatively higher dietary K^+ intake in mice than in humans.

The structural changes along the DCT and CNT may also have significant impact on the handling of ions other than Na^+. Micropuncture and microperfusion experiments reported high transepithelial Ca^{2+} and Mg^{2+} transport rates along the DCT [reviewed in (1,2)]. The marked atrophy of the DCT in NCC−/− mice suggests a marked reduction of the luminal plasma membrane area available for transepithelial cation transport. This might explain the renal Mg^{2+} wasting but seems to be at odds with the reduced urinary Ca^{2+} excretion in NCC-deficient mice, which is thought to result from an increased Ca^{2+} reabsorption in the DCT (see introduction). Micropuncture studies in wild-type and TRPV5-deficient mice demonstrated that intact Ca^{2+} reabsorption in the DC requires the presence of TRPV5 (37). In wild-type mice, the highest abundance of TRPV5 as well as NCX and plasma membrane Ca^{2+}-ATPase (PMCA) is found in the late DCT (27), which remains intact in NCC−/− mice. Thus, the selective atrophy of the early DCT does not necessarily rule out the hypothesis of an increased Ca^{2+} transport in the DCT. However, chronic stimulation of transcellular Ca^{2+} transport would be expected to go along with an enhanced expression of the Ca^{2+} transporting proteins. Indeed, stimulation of distal nephron Ca^{2+} transport by calcitriol is associated with an induction of distal nephron Ca^{2+} transporting proteins (34). Conversely, inhibition of Ca^{2+} reabsorption by targeted deletion of TRPV5 is associated with reduced expression of CB and NCX (37). In the present study, reverse transcription–PCR, Western blot, and immunohistochemistry did not detect any increased abundance of NCX and TRPV5 in kidneys of NCC-deficient mice. Moreover and most important, the *in vivo* micropuncture experiments indicate similar Ca^{2+} reabsorption rates along the DC of wild-type and NCC knockout mice. In mice of both genotypes, fractional Ca^{2+} delivery decreases steeply at DC

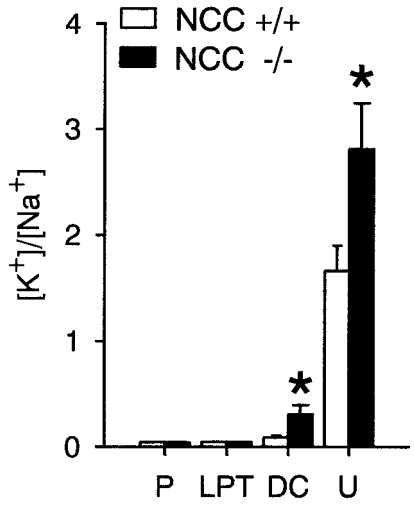

Figure 9. Ratio of K^+ to Na^+ in plasma (P), in fluid of last surface LPT or DC, or in U in NCC+/+ and NCC−/− mice. Values are means ± SEM from seven mice (P and U), 29 to 34 nephrons (LPT), or six to nine nephrons (DC) per group. *$P < 0.05$ *versus* NCC+/+ values.

sites with a low K^+ to Na^+ ratio (presumably late DCT), whereas little further Ca^{2+} reabsorption occurs in DC sites with higher Na^+ *versus* K^+ exchange (presumably CNT; Figure 10). The K^+ to Na^+ ratio increases from the DCT to the end of the CNT as a result of ENaC activity. The observed ion transport profile is consistent with the relative abundance of Ca^{2+} transporting proteins along the late DCT (very high) and CNT (lowered) and strongly suggests unaffected Ca^{2+} transport rates in both segments of NCC –/– mice. Thus, the hypocalciuria is unlikely to be related to altered Ca^{2+} transport along the DC.

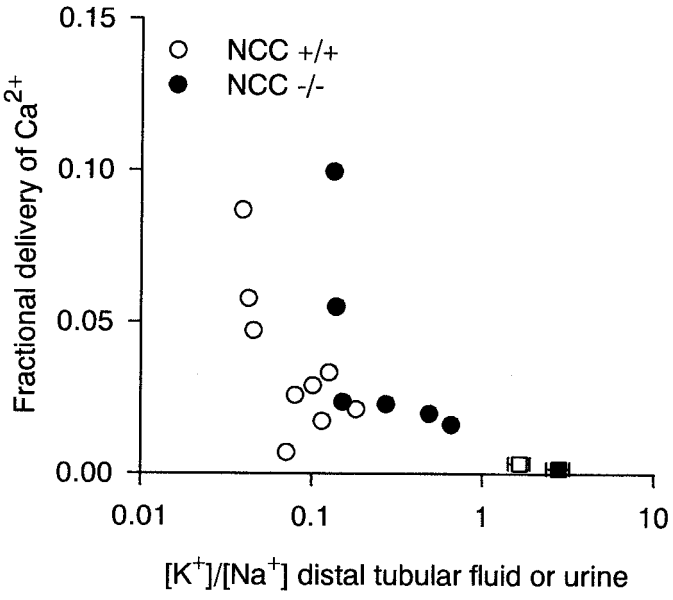

Figure 10. Fractional delivery of Ca^{2+} along DC and in U. Distal luminal K^+ to Na^+ ratio is used as an indicator of the collection site along the DC with lower ratios reflecting earlier collection sites. Circles represent values from single nephrons. Squares ± SEM represent mean values from urine ($n = 7$ per group).

Extracellular volume contraction is a well-known stimulus for paracellular Ca^{2+} reabsorption in the proximal tubules (53). Recent studies by Nijenhuis *et al.* (26) indicated that this mechanism may explain the hypocalciuria induced by chronic thiazide treatment. Thiazide-induced hypocalciuria, present despite drastically downregulated distal tubular Ca^{2+} transporting proteins, was completely prevented by oral replacement of diuresis-related salt and fluid losses (26). NCC-deficient mice have elevated plasma aldosterone concentration, pointing to some degree of extracellular volume depletion. Dietary Na^+ restriction has been reported to aggravate the volume depletion and to augment the hypocalciuria in NCC-deficient mice (23). In the present micropuncture study on mice, the observed hypocalciuria in NCC-deficient mice was the consequence of a reduced GFR and thus lower Ca^{2+} filtration and of an increased fractional proximal reabsorption of Ca^{2+} that was associated with an increased fractional Na^+ reabsorption at this site. The enhanced fractional proximal reabsorption may reflect a primary tubular stimulation but could also, at least in part, be secondary to the reduced GFR, consistent with imperfect glomerulotubular balance. Nevertheless, considering lower fractional Ca^{2+} delivery to the late proximal tubule but similar fractional excretion in urine in NCC knockout than in wild-type mice, the absolute and fractional Ca^{2+} reabsorption downstream of the late proximal tubule, *i.e.*, in the distal nephron segment including the DCT, was actually reduced in mice deficient of NCC (54).

In summary, the genetic loss of NCC function leads to remarkable structural and functional changes in the kidney. Our data provide strong evidence that reduced glomerular filtration and enhanced fractional reabsorption of Na^+ upstream of the DCT and enhanced ENaC-mediated sodium transport downstream of the CNT plays an important role in compensating for the Na^+ transport defect in the DCT. Our data do not provide any support for enhanced Ca^{2+} transport by the DCT but indicate that reduced glomerular filtration and possibly stimulation of proximal reabsorption are causative for the hypocalciuria in NCC-deficient mice and perhaps in patients with Gitelman's syndrome.

Acknowledgments

The study was supported by Swiss National Science Foundation Grants 32-061742.00 and 31-47742.96; the EMDO Foundation; the Stiftung für Wissenschaftliche Forschung an der Universität Zürich; the Cloëtta Foundation; the Institut National de la Santé et de la Recherche Médicale; National Institutes of Health grant DK50594; the Dutch Organization of Scientific Research Grant ZonMw 016.006.001; the Bundesministerium für Bildung, Wissenschaft, Forschung und Technologie (Center for Interdisciplinary Clinical Research) 01 KS 9602; and Deutsche Forschungsgemeinschaft (Va 118/7-2).

Part of this work was presented in 2000 at the ERA-EDTA/EKRA Meeting in Nice (September 17–20, 2000) and the GfN Meeting in Vienna (September 2–5, 2000).

The anti–H-ATPase, anti-NKCC2, and anti-ENaC antibodies were kindly provided by Dr. Steven Gluck, Dr. Steven Hebert, and Dr.

Bernard Rossier, respectively. We thank Lea Kläusli for expert technical assistance with the electron microscopic studies and Dr. M. Le Hir for critical reading of the manuscript.

References

1. Reilly RF, Ellison DH: Mammalian distal tubule: Physiology, pathophysiology, and molecular anatomy. *Physiol Rev* 80: 277–313, 2000
2. Dai LJ, Ritchie G, Kerstan D, Kang HS, Cole DE, Quamme GA: Magnesium transport in the renal distal convoluted tubule. *Physiol Rev* 81: 51–84, 2001
3. Schmitt R, Ellison DH, Farman N, Rossier BC, Reilly RF, Reeves WB, Oberbäumer I, Tapp R, Bachmann S: Developmental expression of sodium entry pathways in rat distal nephron. *Am J Physiol* 276: F367–F381, 1999
4. Loffing J, Pietri L, Aregger F, Bloch-Faure M, Ziegler U, Meneton P, Rossier BC, Kaissling B: Differential subcellular localization of ENaC subunits in mouse kidney in response to high- and low-Na diets. *Am J Physiol Renal Physiol* 279: F252–F258, 2000
5. Biner HL, Arpin-Bott MP, Loffing J, Wang X, Knepper M, Hebert SC, Kaissling B: Human cortical distal nephron: Distribution of electrolyte and water transport pathways. *J Am Soc Nephrol* 13: 836–847, 2002
6. Peng JB, Brown EM, Hediger MA: Epithelial Ca2+ entry channels: Transcellular Ca2+ transport and beyond. *J Physiol* 551: 729–740, 2003
7. Hoenderop JG, Nilius B, Bindels RJ: Molecular mechanism of active Ca2+ reabsorption in the distal nephron. *Annu Rev Physiol* 64: 529–549, 2002
8. Schlingmann KP, Weber S, Peters M, Niemann Nejsum L, Vitzthum H, Klingel K, Kratz M, Haddad E, Ristoff E, Dinour D, Syrrou M, Nielsen S, Sassen M, Waldegger S, Seyberth HW, Konrad M: Hypomagnesemia with secondary hypocalcemia is caused by mutations in TRPM6, a new member of the TRPM gene family. *Nat Genet* 31: 166–170, 2002
9. Voets T, Nilius B, Hoefs S, van der Kemp AWCM, Droogmans G, Bindels RJM, Hoenderop JGJ: TRPM6 forms the Mg2+ influx channel involved in intestinal and renal Mg2+ absorption. *J Biol Chem* 279: 19–25, 2004
10. Wetzel RK, Sweadner KJ: Immunocytochemical localization of Na-K-ATPase alpha- and gamma-subunits in rat kidney. *Am J Physiol Renal Physiol* 281: F531–F545, 2001
11. Simon DB, Nelson-Williams C, Johnson Bia M, Ellison D, Karet FE, Molina AM, Vaara I, Iwata F, Cushner HM, Koolen M, Gainza FJ, Gitelman HJ, Lifton RP: Gitelman's variant of Bartter's syndrome, inherited hypokalaemic alkalosis, is caused by mutations in the thiazide-sensitive Na-Cl cotransporter. *Nat Genet* 12: 24–30, 1996
12. Syren ML, Tedeschi S, Cesareo L, Bellantuono R, Colussi G, Procaccio M, Ali A, Domenici R, Malberti F, Sprocati M, Sacco M, Miglietti N, Edefonti A, Sereni F, Casari G, Coviello DA, Bettinelli A: Identification of fifteen novel mutations in the SLC12A3 gene encoding the Na-Cl Co-transporter in Italian patients with Gitelman syndrome. *Hum Mutat* 20: 78, 2002
13. Reissinger A, Ludwig M, Utsch B, Promse A, Baulmann J, Weisser B, Vetter H, Kramer HJ, Bokemeyer D: Novel NCCT gene mutations as a cause of Gitelman's syndrome and a systematic review of mutant and polymorphic NCCT alleles. *Kidney Blood Press Res* 25: 354–362, 2002
14. De Jong JC, Van Der Vliet WA, Van Den Heuvel LP, Willems PH, Knoers NV, Bindels RJ: Functional expression of mutations in the human NaCl cotransporter: Evidence for impaired routing mechanisms in Gitelman's syndrome. *J Am Soc Nephrol* 13: 1442–1448, 2002
15. Kunchaparty S, Palcso M, Berkamn J, Velazquez H, Desir GV, Bernstein J, Reilly RF, Ellison DH: Defective processing and expression of thiazide-sensitive Na-Cl cotransporter as a cause of Gitelman's syndrome. *Am J Physiol* 277: F643–F649, 1999
16. Cruz DN, Simon DB, Nelson-Williams C, Farhi A, Finberg K, Burleson L, Gill JR, Lifton RP: Mutations in the Na-Cl cotransporter reduce blood pressure in humans. *Hypertension* 37: 1458–1464, 2001
17. Costanzo LS, Windhager EE: Calcium and sodium transport by the distal convoluted tubule of the rat. *Am J Physiol* 235: F497–F506, 1978
18. Lajeunesse D, Brunette MG: The hypocalciuric effect of thiazides: Subcellular localization of the action. *Pflugers Arch* 417: 454–462, 1991
19. Gesek FA, Friedman PA: Mechanism of calcium transport stimulated by chlorothiazide in mouse distal convoluted tubule cells. *J Clin Invest* 90: 429–438, 1992
20. Friedman PA: Codependence of renal calcium and sodium transport. *Annu Rev Physio,* 60: 179–197, 1998
21. Quamme GA, Wong NL, Sutton RA, Dirks JH: Interrelationship of chlorothiazide and parathyroid hormone: A micropuncture study. *Am J Physiol* 229: 200–205, 1975
22. Dai L-J, Friedman PA, Quamme GA: Cellular mechanisms of chlorothiazide and cellular potassium depletion on Mg^{2+} uptake in mouse distal convoluted tubule cells. *Kidney Int* 51: 1008–1017, 1997
23. Schultheis PJ, Lorenz JN, Meneton P, Niema ML, Riddle TM, Flagella M, Duffy JJ, Doetschman T, Miller ML, Shull GE: Phenotype resembling Gitelman's syndrome in mice lacking the apical Na^+-Cl^- cotransporter of the distal convolute tubule. *J Biol Chem* 273: 1–6, 1998
24. Bachmann S, Bostanjoglo M, Schmitt R, Ellison DH: Sodium transport-related proteins in the mammalian distal nephron—Distribution, ontogeny and functional aspects. *Anat Embryol (Berl)* 200: 447–468, 1999
25. Loffing J, Kaissling B: Sodium and calcium transport pathways along the mammalian distal nephron: From rabbit to human. *Am J Physiol Renal Physiol* 284: F628–F643, 2003
26. Nijenhuis T, Hoenderop JG, Loffing J, van der Kemp AW, van Os CH, Bindels RJ: Thiazide-induced hypocalciuria is accompanied by a decreased expression of Ca2+ transport proteins in kidney. *Kidney Int* 64: 555–564, 2003
27. Loffing J, Loffing-Cueni D, Valderrabano V, Klausli L, Hebert SC, Rossier BC, Hoenderop JG, Bindels RJ, Kaissling B: Distribution of transcellular calcium and sodium transport pathways along mouse distal nephron. *Am J Physiol Renal Physiol* 281: F1021–F1027, 2001
28. Kaplan MR, Plotkin MD, Lee W-S, Xu Z-C, Lytton J, Hebert SC: Apical localization of the Na-K-Cl cotransporter, *rBSC1*, on rat thick ascending limbs *Kidney Int* 49: 40–47, 1996
29. Duc C, Farman N, Canessa CM, Bonvalet J-P, Rossier BC: Cell-specific expression of epithelial sodium channel α, β, and γ subunits in aldosterone-responsive epithelia from the rat: Localization by in situ hybridization and immunocytochemistry. *J Cell Biol* 127: 1907–1921, 1994
30. Hoenderop JG, Hartog A, Stuiver M, Doucet A, Willems PH, Bindels RJ: Localization of the epithelial $Ca^{(2+)}$ channel in rabbit kidney and intestine. *J Am Soc Nephrol* 11: 1171–1178, 2000

31. Hemken P, Guo X-L, Wang Z-Q, Zhang K, and Gluck S: Immunologic evidence that vacuolar H^+ ATPases with heterogeneous forms of $M_r = 31{,}000$ subunit have different membrane distributions in mammalian kidney. *J Biol Chem* 267: 9948–9957, 1992
32. Kriz W, Kaissling B: Structural organization of the distal nephron. In: *The Kidney: Physiology and Pathophysiology*, edited by Seldin DW, Giebisch G, Philadelphia, Lippincott, 2000, pp 587–654
33. Weibel ER: *Stereological Methods: Practical Methods for Morphometry*, New York, Academic Press, 1979
34. Hoenderop JG, Müller D, van der Kemp AW, Hartog A, Suzuki M, Ishibashi K, Imai M, Sweep F, Willems PH, van Os CH, Bindels RJ: Calcitriol controls the epithelial calcium channel in kidney. *J Am Soc Nephrol* 12: 1342–1349, 2001
35. Hoenderop JG, Dardenne O, Van Abel M, Van Der Kemp AW, Van Os CH, St-Arnaud R, Bindels RJ: Modulation of renal Ca2+ transport protein genes by dietary Ca2+ and 1,25-dihydroxyvitamin D3 in 25-hydroxyvitamin D3–1α-hydroxylase knockout mice. *FASEB J* 16: 1398–1406, 2002
36. Vallon V, Grahammer F, Richter K, Bleich M, Lang F, Barhanin J, Volkl H, Warth R: Role of KCNE1-dependent K+ fluxes in mouse proximal tubules. *J Am Soc Nephrol* 12: 2003–2011, 2001
37. Hoenderop JG, van Leeuwen JP, van der Eerden BC, Kersten FF, van der Kemp AW, Merillat AM, Warsing JH, Rossier BC, Vallon V, Hummler E, Bindels RJ: Renal Ca^{2+} wasting, hyperabsorption, and reduced bone thickness in mice lacking TRPV5. *J Clin Invest* 112: 1906–1914, 2003
38. Loffing J, Loffing-Cueni D, Hegyi I, Kaplan MR, Hebert SC, Le Hir M, Kaissling B: Thiazide treatment of rats provokes apoptosis in distal tubule cells. *Kidney Int* 50: 1180–1190, 1996
39. Bettinelli A, Bianchetti MG, Girardin E, Caringella A, Cecconi M, Appiani AC, Pavanello L, Gastaldi R, Isimbaldi C, Lama G, *et al.*: Use of calcium excretion values to distinguish two forms of primary renal tubular hypokalemic alkalosis: Bartter and Gitelman syndromes. *J Pediatr* 120: 38–43, 1992
40. Weinman EJ, Eknoyan G: Chronic effects of chlorothiazide on reabsorption by the proximal tubule of the rat. *Clin Sci Mol Med* 49: 107–113, 1975
41. Brooks H, Sorensen A, Terris J, Schultheis P, Lorenz J, Shull G, Knepper M: Profiling of renal tubule Na^+ transporter abundances in NHE3 and NCC null mice using targeted proteomics. *J Physiol* 530: 359–366, 2001
42. Masilamani S, Kim GH, Mitchell C, Wade JB, Knepper MA: Aldosterone-mediated regulation of ENaC alpha, beta, and gamma subunit proteins in rat kidney. *J Clin Invest* 104: R19–R23, 1999
43. Verrey F, Hummler E, Schild L, Rossier BC: Control of Na+ transport by aldosterone. In: *The Kidney—Physiology and Pathophysiology*, 3rd Ed., edited by Seldin W, Giebisch G, Philadelphia, Lippincott Williams & Wilkins, 2000, pp 1441–1471
44. Wade JB, Stanton BA, Field MJ, Kashgarian M, Giebisch G: Morphological and physiological responses to aldosterone: time course and sodium dependence. *Am J Physiol* 259: F88–F94, 1990
45. Kaissling B, Le Hir M: Distal tubular segments of the rabbit kidney after adaptation to altered Na- and K-intake. I. Structural changes. *Cell Tissue Res* 224: 469–492, 1982
46. Loffing J, Zecevic M, Feraille E, Kaissling B, Asher C, Rossier BC, Firestone GL, Pearce D, Verrey F: Aldosterone induces rapid apical translocation of ENaC in early portion of renal collecting system: Possible role of SGK. *Am J Physiol Renal Physiol* 280: F675–F682, 2001
47. Frindt G, Palmer LG: Na channels in the rat connecting tubule. *Am J Physiol Renal Physiol* 286: F669–F674, 2004
48. Almeida AJ, Burg MB: Sodium transport in the rabbit connecting tubule. *Am J Physiol* 243: F330–F334, 1982
49. Tomita K, Pisano JJ, Knepper MA: Control of sodium and potassium transport in the cortical collecting duct of the rat. *J Clin Invest* 76: 132–136, 1985
50. Reif MC, Troutman SL, Schafer JA: Sodium transport by rat cortical collecting tubule: Effects of vasopressin and deoxycorticosterone. *J Clin Invest* 77: 1291–1298, 1986
51. Rubera I, Loffing J, Palmer LG, Frindt G, Fowler-Jaeger N, Sauter D, Carroll T, McMahon A, Hummler E, Rossier BC: Collecting duct-specific gene inactivation of αENaC in the mouse kidney does not impair sodium and potassium balance. *J Clin Invest* 112: 554–565, 2003
52. Colussi G, Rombola G, De Ferrari ME, Macaluso M, Minetti L: Correction of hypokalemia with antialdosterone therapy in Gitelman's syndrome. *Am J Nephrol* 14: 127–135, 1994
53. Seldin DW: Renal handling of calcium. *Nephron* 81: 2–7, 1999
54. Campean V, Kricke J, Ellison D, Luft FC, Bachmann S: Localization of thiazide-sensitive $Na^{(+)}$-$Cl^{(-)}$ cotransport and associated gene products in mouse DCT. *Am J Physiol Renal Physiol* 281: F1028–F1035, 2001.